Lawrence Berkeley National Laboratory
Recent Work

**Title**
Near atomically smooth alkali antimonide photocathode thin films

**Permalink**
https://escholarship.org/uc/item/927187ht

**Journal**
Journal of Applied Physics, 121(4)

**ISSN**
0021-8979

**Authors**
Feng, J
Karkare, S
Nasiatka, J
et al.

**Publication Date**
2017-01-28

**DOI**
10.1063/1.4974363

Peer reviewed

eScholarship.org
Powered by the California Digital Library
University of California

# Near Atomically Smooth Alkali Antimonide Photocathode Thin Films

Jun Feng,[1, a] Siddharth Karkare,[1] James Nasiatka,[1] Susanne Schubert,[1] John Smedley,[2] and Howard Padmore[1]

[1] *Lawrence Berkeley National Laboratory, Berkeley, CA, USA, 94720*

[2] *Brookhaven National Laboratory, Upton, NY, USA, 11973*

Nano-roughness is one of the major factors degrading the emittance of electron beams that can be generated by high efficiency photocathodes, such as the thermally reacted alkali antimonide thin films. In this paper we demonstrate a co-deposition based method for producing alkali antimonide cathodes that produces near atomic smoothness with high reproducibility. We calculate the effect of the surface roughness on the emittance and show that such smooth cathode surfaces are essential for operation of alkali antimonide cathodes in high field, low emittance radio frequency electron guns and to obtain ultracold electrons for ultrafast electron diffraction applications.

[a] Electronic mail: fjun@lbl.gov

## I. INTRODUCTION

Photoemission based electron sources for the next generation high repetition rate, high brightness x-ray light sources such as Energy Recovery Linacs[1] and Free Electron Lasers[2] need to satisfy several criteria, namely: high (>1%) quantum efficiency (QE) in the visible range, smallest possible intrinsic emittance, fast (sub-ps) response time and a long operational lifetime. During the past decade, alkali-antimonides (eg. $K_2CsSb$) have emerged as the only class of materials that satisfies all these requirements with a high QE >5% and a low intrinsic emittance in the range of 0.36-0.5 $\mu$m per mm rms laser spot size in green (520-545 nm) light[3–5]. Additionally, when operated near the photoemission threshold, alkali-antimonides also show promise as sources of ultra-cold electrons[6] for ultrafast electron diffraction[7] applications and Inverse Compton Scattering based Gamma ray sources[8].

Although alkali antimonides have many excellent characteristics as photoemitters, the synthesis process leads to relatively high levels of surface roughness[9]. Rough cathode surfaces can degrade the intrinsic emittance and make them unusable in electron guns with high electric fields. $K_2CsSb$ photocathodes are typically grown as thin films over conducting substrates by thermal evaporation of ~10-30 nm of Sb followed by sequential thermal evaporation and reaction of K and Cs respectively[3,10]. The films created by this process are not ordered and can have a root mean square (rms) surface roughness as high as 25 nm with a period of roughly 100 nm[9]. Such a surface roughness can distort the electric field near the cathode surface causing the intrinsic emittance to drastically increase. In RF/SRF based electron guns, used for high bunch charge and low emittance applications, the electric field at the cathode surface can be greater than 20 MV/m. In this case the electric field enhancement of the intrinsic emittance can be as high as 1 $\mu$m per mm rms laser spot size making these cathodes unusable[13].

The smallest possible intrinsic emittance is limited by the lattice temperature of the cathode and can be obtained by exciting electrons with near threshold photons[14]. At room temperature, this emittance is 0.22 $\mu$m per mm rms laser spot size. It is possible to reduce this further by cryo-cooling the cathode[6]. However, in alkali-antimonides the smallest possible emittance is limited to a higher value even at photoemission threshold because of the surface roughness[6]. In order to reach the thermal limit and attain the smallest possible intrinsic emittance from cryo-cooled alkali antimonide cathodes a sub-nm surface roughness

would be required[6].

Apart from the surface roughness, another drawback of the traditional sequential growth procedure is its irreproducibility and unreliability. Despite the wide use of this growth technique for streak camera and photomultiplier applications since the 1960s[15,16], this growth technique is complex and remains extremely sensitive to many deposition parameters such as substrate and source temperature, growth rate, final thickness and the quality of vacuum, etc. making it difficult to control and reproduce[17]. The complexity of this technique makes it difficult to automate and the results depend strongly on the skill of the cathode grower[18].

Recently, X-ray diffraction studies have shown that this surface roughness and the irreproducibility in this traditional growth process can be attributed to the exothermic reaction of K (or other alkali metals) deposited on top of the Sb thin film[9,10,19]. This reaction leads to several meta-stable K-Sb phases, making the process difficult to control.

In this paper, we report a procedure to grow K-Cs-Sb cathodes using a co-deposition technique. We present atomic force microscopy measurements and show that this technique produces nearly atomically smooth thin films which will dramatically reduce the emittance growth due to the surface electric field deformations allowing the use of these cathodes in low emittance RF guns and generation of ultra-cold electrons from these cathodes. This growth technique avoids the exothermic reaction between a previously deposited Sb film and alkali metals making it very reproducible and is less complicated than the traditional sequential deposition technique.

In section 2, we describe the experimental setup and the triple-element co-deposition growth process. In section 3 we compare the spectral response, intrinsic emittance and the surface morphology of cathode thin films grown using the traditional sequential deposition and the co-deposition method. The surface morphology is measured using an ultra high vacuum atomic force microscope (UHV-AFM). In section 4 we present a methodology to calculate the effect of electric field and surface roughness on the intrinsic emittance for any given surface. We calculate this effect for the surfaces obtained by the two growth methods and show that the co-deposition technique produces surfaces that can allow the use of alkali antimonides in RF guns with low emittance and can also allow generation of ultra-cold electron beams.

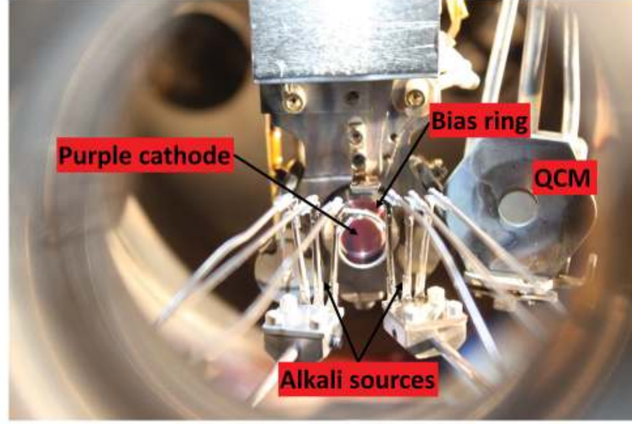


FIG. 1. Picture of the co-deposited cathode along with the alkali metal sources mounted in the UHV deposition chamber

## II. GROWTH CHAMBER AND THE CO-DEPOSITION PROCESS

The UHV deposition chamber has a base pressure in the $10^{-10}$ torr range. The deposition is carried out on the substrate located roughly at the center of the chamber. Sb is evaporated by heating 99.9999% pure Sb pellets (obtained from Alfa Aesar[20]) in a ceramic furnace. A pre-calibrated quartz crystal microbalance (QCM) is used to measure the Sb deposition rate. The alkali metals are simultaneously evaporated from 17 mm getter sources manufactured by SAES[21]. The alkali metal sources are mounted 30 mm away from the substrate as shown in figure 1. The substrate is grounded and a bias ring (biased to 30-50 V) is used to collect the photocurrent emitted from the cathode during and after deposition to measure the QE.

Several photocathodes were prepared on Mo and Si substrates, 10-12 mm in diameter. The surface of the substrates was optically polished and heated to 200-400°C for 30 minutes in a UHV deposition chamber for cleaning prior to growth. The Si substrates were $n$-doped with Phosphorus to ensure semi-metallic behavior. No significant substrate dependence was found. The substrate temperature is maintained at 90°C during the entire deposition process. The high substrate temperature is required to achieve the reaction between antimony and the alkali metals[19].

Sb, K and Cs are deposited simultaneously on the substrate. Sb is deposited at a rate of 0.1Å/s as measured by the QCM. This assumes a sticking coefficient of 1, as demonstrated by cross calibration with x-ray reflectivity and scanning electron microscopy measurements[23].

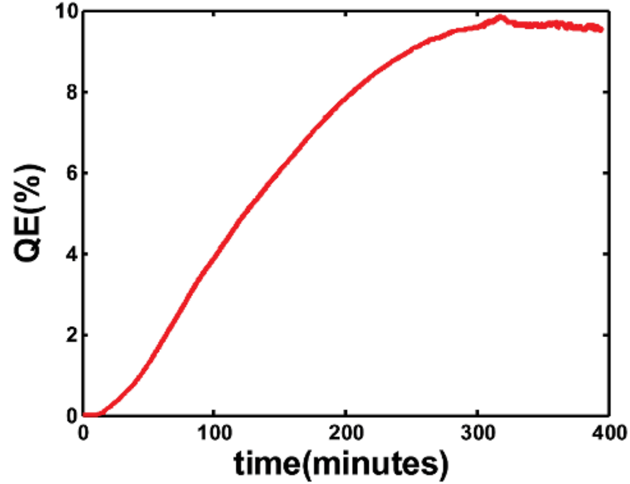


FIG. 2. QE of the K-Cs-Sb cathode grown using the co-deposition process as a function of growth time at 532 nm incident photon wavelength

The alkali metals are evaporated by passing currents of 4.7 A and 5.5 A through the K and Cs sources respectively. No parameter needs to be varied during the entire process. The deposition rate of K and Cs cannot be similarly measured using a QCM due to the unknown sticking coefficients of the alkali metals on the QCM and variability caused by temperature and deposition history[24].

A 532 nm laser is used to monitor the QE during deposition. Figure 2 shows the QE as a function of deposition time. It can be seen that the cathode growth is very smooth and no tweaking of the sources is required during growth. Evaporation of all the three metals is started simultaneously. The deposition rate is held constant throughout the deposition process. As seen from figure 2, the QE starts to increase about 9 minutes after starting the deposition process and continues to increase up to 10% in roughly 300 mins. At this point the QE reaches a maxima and then saturates. All the sources are turned off at this point and the substrate is allowed to cool. The QE stays nearly constant as the substrate cools down slowly to room temperature. If the deposition is continued beyond this point, the QE does not reduce as in the case of sequential deposition. Instead it remains constant at the maximum value. Ten cathodes were grown using this procedure and all gave a final QE between 5-10%.

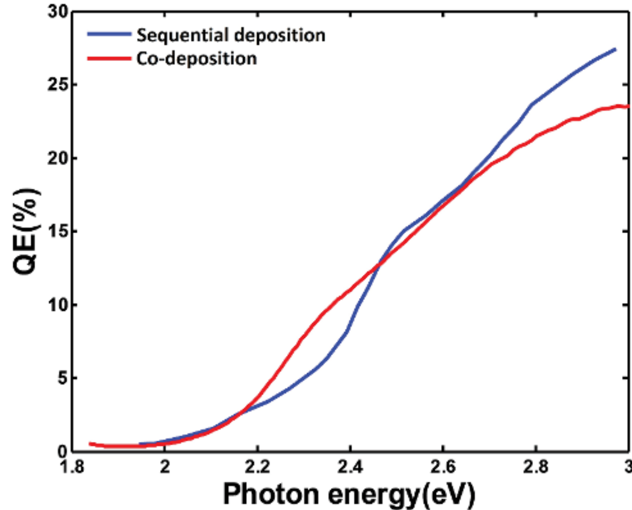


FIG. 3. Comparison of the spectral response of the K-Cs-Sb cathodes grown by co-deposition and sequential deposition techniques

## III. CATHODE CHARACTERIZATION

### A. Spectral Response

The spectral response of the K-Cs-Sb cathode is measured using a plasma based wavelength tunable light source[25]. Figure 3 shows a comparison of the K-Cs-Sb cathodes grown using the co-deposition process and the traditional sequential growth process[4]. We can see that cathodes grown using both techniques have nearly the same photoemission threshold, but the QE of the co-deposition cathode is higher between photon energies of 2.2 eV and 2.4 eV and is lower at photon energies greater than 2.6 eV. These differences can be attributed to possible structural and compositional differences between the cathodes obtained by the two deposition techniques.

### B. Intrinsic Emittance

The intrinsic emittance of the cathodes grown using the co-deposition technique was measured using an acceleration-drift method[26] and a solenoid scan technique[3] at low electric fields (∼1 MV/m). The intrinsic emittance was found to be $0.39\pm0.04$ $\mu$m per mm rms laser spot size at 532 nm. This is the same as the value of $0.36\pm0.04$ $\mu$m per mm rms laser spot size measured for the sequential deposition technique[4] within the experimental error.

At 532 nm and a surface electric field of 1 MV/m the emittance is dominated by the excess energy of the electrons and not by the surface induced electric field deformations[3]. Hence the emittance measured from cathodes grown using both recipes is identical.

### C. Surface Roughness

Surface morphology of the cathodes was measured using a RHK UHV-AFM[22] connected in vacuum to the growth chamber.

In order to compare the surface roughness, two cathodes were grown - one using the co-deposition technique described above and the other using a sequential growth technique[4] on commercially bought Si substrates with roughness below 0.3 nm. These cathodes were then transported in vacuum into an UHV-AFM. The thickness of the initial Sb layer for the sequential deposition was 7 nm.

Figures 4 (a) and (b) shows the AFM images of the cathodes grown using the sequential and the co-deposition processes respectively. It can be seen that the cathode grown using the sequential growth procedure has a much larger roughness amplitude. The rms surface roughness of the cathode is 2.5 nm and the average spacing between nearest neighbor peaks is $\sim$ 100 nm. The cathode grown using the co-deposition techniques is much smoother with an rms roughness of 0.6 nm and average spacing between nearest neighbor peaks of $\sim$ 40 nm.

## IV. EFFECT OF ROUGHNESS ON EMITTANCE

A rough surface can increase the emittance in two ways[11,12] - (a) Slope effect and (b) Field effect. The slope effect refers to the increase in emittance because the electrons are emitted about the local surface normal and not the global surface normal. This effect is dominant when the emission of electrons is highly directed[11]. Due to the disorder on the surface the emission from alkali antimonide cathodes is assumed to be isotropic making the slope effect negligible. The field effect refers to the emittance increase because of the distortion of electric field close to the rough surfaces.

Ignoring the contribution of the slope effect, the intrinsic emittance after accounting for

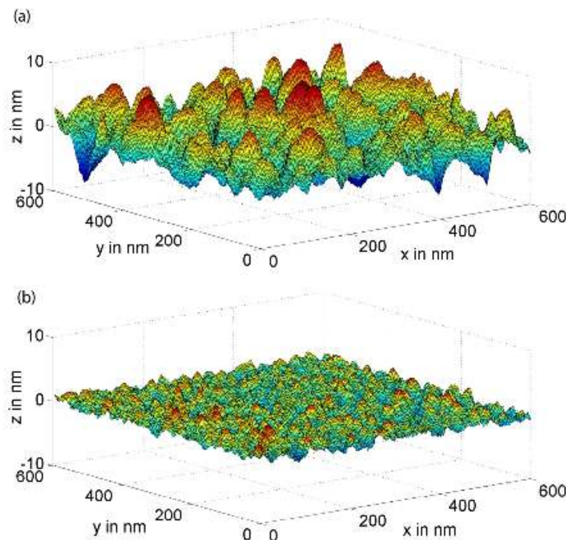


FIG. 4. (a) AFM image of a cathode grown using sequential deposition (b) AFM image of a cathode grown using the co-deposition technique

the electric field effect to first order can be given by

$$\epsilon_{in} = \sqrt{\epsilon_{in0}^2 + \epsilon_f^2}, \tag{1}$$

where $\epsilon_{in0}$ is the intrinsic emittance of the cathode at near zero electric field and $\epsilon_f$ is the enhancement to the intrinsic emittance at an longitudinal electric field of $f$ MV/m (typically in the range of 1-20 MV/m) at the cathode surface.

Let us assume $z$ to be the co-ordinate along the global normal to the surface and the direction of electron beam propagation, and $x$ and $y$ to be the co-ordinates transverse to the direction of beam propagation. For a simple 1-D sinusoidal roughness on the cathode surface given by $z = A\cos\left(\frac{2\pi x}{p}\right)$, when the amplitude $A$ is much smaller than the period $p$, the field effect enhancement in emittance (per unit laser spot size) can be easily calculated as[12,13]

$$\epsilon_f = \sqrt{\frac{\pi^2 A^2 E_0 e}{2 m_e c^2 p}} \tag{2}$$

where $A$ is the amplitude of the roughness, $p$ is the period, $E_0$ is the longitudinal electric field at the cathode surface, $m_e$ is the electron rest mass and $c$ is the speed of light. We see that $\epsilon_f$ is directly proportional to the amplitude of the roughness and to the square root of the longitudinal electric field at the surface and is inversely proportional to the period of the roughness. Equation 2 is useful in terms of understanding the scaling of the electric

field enhancement with the surface roughness parameters (the amplitude $A$ and the period $p$) and the longitudinal electric field ($E_0$) away from the cathode surface, however, it cannot calculate accurately the electric field enhancement from realistic 2-D rough surfaces as shown in figure 4.

In order to calculate $\epsilon_f$ for any given realistic 2-D surface, the surface can be expanded in its 2-D Fourier components and can be written as

$$z = \sum_m \sum_n A_{m,n} \phi_{m,n}(x, y) \tag{3}$$

where $A_{m,n}$ are the Fourier coefficients and $\phi_{m,n} = \cos\left(\frac{2\pi x}{p_m} + \alpha_m\right)\cos\left(\frac{2\pi y}{p_n} + \alpha_n\right)$ are 2-D sinusoidal functions. $p_m$ and $p_n$ are periods of the sinusoidal functions in the $x$ and $y$ directions respectively and $\alpha_m$ and $\alpha_n$ are the phases of the sinusoidal functions in the $x$ and $y$ directions respectively. Assuming that the surface is conducting and the electric field lines are perpendicular to the local surface, the electric potential near the surface can be given by[27]

$$U = E_0 z + \sum_m \sum_n C_{m,n} e^{z/p_{m,n}} \phi_{m,n}(x, y) \tag{4}$$

where $p_{m,n}^{-1} = \sqrt{p_m^{-2} + p_n^{-2}}$. The coefficients $C_{m,n}$ are calculated numerically to ensure that the potential given by equation 4 is constant over the 2-D rough surface[27] given by equation 3. If $p_{m,n} \gg A_{m,n}$ then $C_{m,n} \approx A_{m,n} E_0$[12].

Assuming the transverse position to be nearly constant during the acceleration one can calculate the velocity change in the $x$ direction due to the electric field as

$$v_{fx} = \frac{e}{2m_e} \sum_m \sum_n C_{m,n} \frac{d\phi_{m,n}}{dx} \sqrt{\frac{2\pi m_e p_{m,n}}{eE_0}}. \tag{5}$$

The electric field enhancement of emittance (per unit laser spot size) in the $x$ direction can be calculated as

$$\epsilon_f = \frac{\sqrt{\langle m_e^2 v_{xf}^2 \rangle}}{m_e c} \tag{6}$$

From equations 5 and 6, one can easily calculate the enhancement in intrinsic emittance (per unit laser spot size) as

$$\epsilon_f = \sqrt{\frac{e\pi^2}{2m_e c^2 E_0} \sum_m \sum_n C_{m,n}^2 p_{m,n} / p_m^2}. \tag{7}$$

Note that since $C_{m,n}$ is directly proportional to $E_0$ and $A_{m,n}$, the scaling relations of $\epsilon_f$ with the surface roughness parameters and the electric field obtained for the 1-D sinusoidal surface still hold. Also, note that for a 1-D sinusoidal surface equation 7 reduces to equation 2.

The surfaces shown in figure 4 were expressed in terms of their 2-D Fourier components as in equation 3. The maximum period that can be used in the Fourier expansion is the size of the measured surface in $x$ and $y$ directions. For the surfaces shown in figure 4 the size of the measured surface is 600 nm in both $x$ and $y$ directions. It was found that considering the first 30 harmonics in each direction for the Fourier expansion is sufficient to model the surfaces accurately. Thus the values of the periods $p_m$ and $p_n$ are given as $600/m$ nm and $600/n$ respectively. Here both $m$ and $n$ range from 0 to 30. After expressing the surfaces in terms of their Fourier components, the coefficients $C_{m,n}$ can be calculated numerically by enforcing the surface to be equipotential[27]. Once the $C_{m,n}$ coefficients are known it is straightforward to calculate $\epsilon_f$ from equation 7. The electric field enhancements calculated using the above formalism for the two surfaces shown in figure 4 at electric fields of 5 MV/m ($\epsilon_5$), 20 MV/m ($\epsilon_{20}$) and 100 MV/m ($\epsilon_{100}$) is shown in table I.

Electric fields in VHF RF photoguns[28] can be as high as 20 MV/m and in low frequency RF guns can be as high as 100 MV/m. For the high field guns (100 MV/m) we can see that the roughness induced electric field enhancements of the emittance generated from the rough sequentially evaporated cathode is 0.8 $\mu$m/mm rms, well above the low field intrinsic emittance ($\epsilon_{in0}$) of $\sim$ 0.35-0.5$\mu$m/mm rms in green light. The smooth surface obtained from the co-deposition technique gives an electric field enhancement of only 0.31 $\mu$m/mm rms, which is still smaller than the low field intrinsic emittance, making such smooth surfaces desirable for low emittance operation.

The smallest possible low field intrinsic emittance ($\epsilon_{in0}$) is limited by the lattice temperature to 0.22 $\mu$m/mm rms at room temperature and to 0.12 $\mu$m/mm rms at 100 K . The electric field enhancement at 20 MV/m for the rough surface is 0.36 $\mu$m/mm rms, well above the thermally limited intrinsic emittance at room temperature. The electric field enhancement in cryo-cooled DC guns (with electric field of $\sim$ 5 MV/m) is as high as 0.18 $\mu$m/mm rms, well above the thermally limited intrinsic emittance at 100 K. The smooth surface obtained from the co-deposition technique gives an enhancement of only 0.07 $\mu$m/mm rms at 5 MV/m and 0.14 $\mu$m/mm rms at 20 MV/m, allowing the production of ultracold electrons

| Quantity | Sequential deposition | Co-deposition |
|---|---|---|
| RMS roughness (nm) | 2.5 | 0.6 |
| $\epsilon_5$ ($\mu$m/mm rms) | 0.18 | 0.07 |
| $\epsilon_{20}$ ($\mu$m/mm rms) | 0.36 | 0.14 |
| $\epsilon_{100}$ ($\mu$m/mm rms) | 0.80 | 0.31 |

TABLE I. RMS roughness and the calculated enhancement in emittance for electric fields of 5 MV/m, 20 MV/m and 100 MV/m for the two surfaces shown in figure 4

using cryo-cooled cathodes.

## V. CONCLUSION

In conclusion we have demonstrated a triple element co-deposition based technique to grow ultrasmooth alkali-antimonide cathodes. The technique is significantly simpler than the traditional sequential methodology, easily reproducible and can lead to the automation of the growth process of alkali antimonide cathode. Additionally, this technique produces cathodes with sub-nm scale roughness allowing their use in high bunch charge applications where electric fields at the cathode exceed 20 MV/m without significant degradation in intrinsic emittance. In theory, the surface roughness is small enough to allow production of ultra-cold electron beams from alkali-antimonide cathodes enabling futuristic applications of these cathodes. However, in practice, production of ultra-cold electrons may still be limited by other effects like work function non-uniformities and surface defects[29]. The stoichiometry and structure of the material obtained by this technique is still under investigation.

This work was performed at LBNL under the auspices of the Office of Science, Office of Basic Energy Sciences, of the U.S. Department of Energy under Contract No. DE-AC02-05CH11231, KC0407-ALSJNT-I0013, and DE-SC0005713

## REFERENCES

[1]S. M. Gruner, D. Bilderback, I. Bazarov, K. Finkelstein, G. Krafft, L. Merminga, H. Padamsee, Q. Shen, C. Sinclair, and M. Tigner, Rev. Sci. Instr. **73**, 1402 (2002).

[2]P. Emma, R. Akre, J. Arthur, R. Bionta, C. Bostedt, J. Bozek, A. Brachmann, P. H. Bucksbaum, R. Coffee, F. J. Decker, *et al.*, Nat. Photonics **4**, 641 (2010).

[3]I. Bazarov, L. Cultrera, A. Bartnik, B. Dunham, S. Karkare, Y. Li, X. Liu, J. Maxson, and W. Roussel, Appl. Phys. Lett. **98**, 224101 (2011).

[4]T. Vecchione, I. Ben-Zvi, D. H. Dowell, J. Feng, T. Rao, J. Smedley, W. Wan, and H. A. Padmore, Appl. Phys. Lett. **99**, 034103 (2011).

[5]B. Dunham, J. Barley, A. Bartnik, I. Bazarov, L. Cultrera, J. Dobbins, G. Hoffstaetter, B. Johnson, R. Kaplan, S. Karkare, *et al.*, Appl. Phys. Lett. **102**, 034105 (2013).

[6]L. Cultrera, S. Karkare, H. Lee, X. Liu, I. Bazarov, and B. Dunham, Phys. Rev. ST - Acc. Beams **18**, 113401 (2015).

[7]P. Musumeci, J. T. Moody, C. M. Scoby, M. S. Gutierrez, H. A. Bender, and N. S. Wilcox, Rev. Sci. Instr. **81**, 013306 (2010).

[8]S. Boucher, P. Frigola, A. Murokh, M. Ruelas, I. Jovanovic, J. Rosenzweig, and G. Travish, Nucl. Instr. Meth. A **608**, S54 (2009).

[9]S. Schubert, M. Ruiz-Oses, I. Ben-Zvi, T. Kamps, X. Liang, E. Muller, K. Mueller, H. Padmore, T. Rao, X. Tong, T. Vecchione, and J. Smedley, APL-Materials **1**, 032119 (2013).

[10]M. Ruiz-Oses, S. Schubert, K. Attenkofer, I. Ben-Zvi, X. Liang, E. Muller, H. Padmore, T. Rao, T. Vecchione, J. Wong, J. Xie, and J. Smedley, APL-Materials **2**, 121101 (2014).

[11]S. Karkare and I. Bazarov, Appl. Phys. Lett. **98**, 094104 (2011).

[12]D. J. Bradley, M. B. Allenson, and B. R. Holeman, J. Phys. D: Appl. Phys. **10**, 111 (1977).

[13]J. Smedley, M. Gaowei, J. Sinsheimer, K. Attenkofer, J. Walsh, S. Schubert, J. Wong, H. Padmore, J. Kuhn, E. Muller, Z. Ding, H. Frisch, H. B. Bhandari, H. Lingertat, V. Wang, O. Ovechkina, and V. V. Nagarkar, Proceedings of IPAC 2015 , TUPHA003 (2015).

[14]J. Feng, J. Nasiatka, W. Wan, S. Karkare, J. Smedley, and H. Padmore, Appl. Phys. Lett. **107**, 134101 (2015).

[15]A. Sommer, Appl. Phys. Lett. **3**, 62 (1963).

[16]M. Kapusta, P. Lavoute, F. Lherbet, E. Rossignol, C. Moussant, and F. Fouche, IEEE Nuclear Science Symposium Conference Record **1**, 73 (2007).

[17]D. Dowell, S. Bethel, and K. Friddell, Nucl. Instrum. Methods A **356**, 167 (1995).

[18]K. Nakamura, Y. Hamana, Y. Ishigami, and T. Matsui, Nucl. Instrum. Methods A **623**,

276 (2010).

[19]S. Schubert, J. Wong, J. Feng, S. Karkare, H. Padmore, M. Ruiz-Oses, J. Smedley, E. Muller, Z. Ding, M. Gaowei, *et al.*, J. Appl. Phys. **In print** (2016).

[20]`https://www.alfa.com/en/`.

[21]`https://www.saesgetters.com/`.

[22]`http://www.rhk-tech.com/products/beetle-uhv-vt-afm/`.

[23]X. Liang, M. Ruiz-Oss, I. Ben-Zvi, J. Smedley, K. Attenkofer, T. Vecchione, H. Padmore, and S. Schubert, Proceedings of IPAC 2012 , MOPPP049 (2012).

[24]A. W. Czanderna, C. J. Powell, and T. E. Madey, *Specimen Handling, Preparation, and Treatments in Surface Characterization* (Kluwer Academic Publishers, New York).

[25]J. Feng, J. Nasiatka, J. Wong, X. Chen, S. Hidalgo, T. Vecchione, H. Zhu, F. J. Palomares, and H. A. Padmore, Rev. Sci. Instrum. **84**, 085114 (2013).

[26]J. Feng, J. Nasiatka, W. Wan, T. Vecchione, and H. A. Padmore, Rev. Sci. Instrum. **86**, 015103 (2015).

[27]T. Gorlov, Journal of Electrostatics **65**, 735 (2007).

[28]F. Sannibale, J. Doyle, J. Feng, D. Filippetto, S. Gierman, G. Harris, M. Johnson, T. Kramasz, D. Leitner, R. Li, *et al.*, Proceedings of IPAC 2016 , TUOCA02 (2016).

[29]S. Karkare and I. Bazarov, Phys. Rev. Applied **4**, 024015 (2015).